# Structure and Dynamics of Nonionic Surfactant Aggregates in Layered Materials

Régis Guégan, Emmanuel Véron, Lydie Le Forestier, Makoto Ogawa, Sylvian Cadars

## HAL Id: insu-01609051
## https://insu.hal.science/insu-01609051

# Structure and Dynamics of Nonionic Surfactant Aggregates in Layered Materials

*Régis Guégan,[†,*] Emmanuel Veron,[‡] Lydie Le Forestier,[†] Makoto Ogawa[§], and Sylvian Cadars[‡,¶,*]*

[†]ISTO, UMR 7327 CNRS-Université d'Orléans, 1A Rue de la Férollerie, 45071 Orléans Cedex 2, France

[‡]CEMHTI CNRS UPR3079, Université d'Orléans, 1D avenue de la recherche-scientifique, 45071 Orléans Cédex 2, France

[§] School of Energy Science and Engineering, Vidyasirimedhi Institute of Science and Technology, Rayong 21210, Thailand

[¶] Institut des Matériaux Jean Rouxel (IMN), Université de Nantes, CNRS, 2 Rue de la Houssinière, BP32229, 44322 Nantes Cedex 3, France

*To whom correspondence should be addressed: E-mail: regis.guegan@univ-orleans.fr. Phone: +33 (0) 2 38 49 25 41. Fax: +33 (0) 2 38 63 64 88, E-mail Sylvian.Cadars@cnrs-imn.fr.

ABSTRACT

Aggregation of surfactants on solid surfaces as they are adsorbed from solution is the basis of numerous technological applications such as colloidal stabilization, ore flotation, or cleaning floors. The understanding of both the structure and the dynamics of surfactant aggregates for the development of alternative way of preparation of hybrid layered materials. For this purpose, we study the adsorption of the tri-ethylene glycol mono n-decyl ether ($C_{10}E_3$) nonionic surfactant onto a synthetic montmorillonite (Mt), an aluminosilicate clay mineral for organoclay preparation with important applications in materials sciences, catalysis, wastewater treatment, or as drug delivery. The aggregation mechanisms follow those observed in an analogous natural Mt, with the condensation of $C_{10}E_3$ in a bilayer arrangement once the surfactant self-assembles in a lamellar phase beyond the critical micelle concentration, underlining the importance of the surfactant state in solution. Solid-state $^1H$ nuclear magnetic resonance (NMR) at fast magic-angle spinning (MAS) and high magnetic field, combined with $^1H$-$^{13}C$ correlation experiments and different types of $^{13}C$ NMR experiments selectively probe mobile or rigid moieties of $C_{10}E_3$ in three different aggregate organizations: (i) lateral monolayer, (ii) lateral bilayer, and (iii) normal bilayer. High-resolution $^1H\{^{27}Al\}$ CP-$^1H$-$^1H$ spin diffusion experiments shed light on proximities and dynamics of the dynamics of different fragments and fractions of the intercalated surfactant molecules with respect to the Mt surface. $^{23}Na$ and $^1H$ NMR measurements combined with complementary NMR data, at both molecular and nanometer scales, precisely pointed out the location $C_{10}E_3$ ethylene oxide hydrophilic group in close contact with Mt surface interacting through ion-dipole or Van der Waals interactions.

KEYWORDS: NMR, surfactants, adsorption, hybrid materials, organoclays, smectite, layered alumino-silicates, 2:1 clays.

# Introduction

An important feature of amphiphilic molecules is their ability to form ordered aggregates on interfaces.[1,2] Numerous studies have shown that aggregate structures assembled on various solid surfaces could be similar to those existing in bulk solution with some differences.[3] Aggregation mechanisms on solid surfaces, which determine many technological applications such as colloidal stabilization, ore flotation, or cleaning floors, differ from bulk solution by involving additional forces with the surface. This often results in differences in how the surfactant self-arranges by optimizing the organization of micelles onto a surface.[4] The aggregate structures thus formed depend on the nature of the solid surface (homogenous and/or heterogeneous, hydrophobicity and/or hydrophilicity, charge density), the kind of surfactant (ionic or not), and its bulk form (single molecules/liquid crystalline phases).

Clay minerals such as montmorillonite (Mt) are layered materials whose layers consist of one octahedral sandwiched by two tetrahedral sheets (structure 2:1). Isomorphic substitutions usually occurs in octahedral sheets leading to a negative net charge of the surface which is counterbalanced by the presence of inorganic cations, easily exchangeable, within the interlayer space.[5-9] Thus, cationic surfactants can be adsorbed/intercalated by replacing site by site the exchangeable inorganic cations through electrostatic interaction excluding any direct micelle aggregation to clay surface.[10] In contrast, the adsorption of nonionic surfactants implies different interaction mechanisms such as: H-bonds, ion-dipole interaction, which preponderance in the adsorption is still a subject of debate of.[11-14] [15] Moreover, these driving adsorption forces display equivalent order of magnitude to those ensuring the cohesion of micelles, thus allowing their possible aggregation to Mt surface. Past aggregation of a lamellar phase of a tri-ethylene glycol mono decyl-n-decyl ether ($C_{10}E_3$) nonionic surfactant onto a montmorillonite (Mt) confirmed the importance of the surfactant state between single molecules and liquid crystalline phase.[16-18] These previous works could not precisely stress out the main driving force (H-bonds and ion-dipole interaction) due to impurities (ferromagnetic species…) and the resolution of the traditional techniques used in the characterization of hybrid materials based on clay minerals.

Solid-state nuclear magnetic resonance (NMR) represents a powerful tool to probe both the conformation and the dynamics of organic phases at interfaces.[10, 19-30] More particularly, the recent methodological developments have given a fundamental role to the ^{1}H NMR for the characterization of hybrid materials.[31] [5,32] The excellent resolution due to the use of high magnetic fields coupled with multiple pulse magic angle spinning (MAS) sequences lead to a significant reduction of peak broadening caused by homo-nuclear [1]H-^{1}H dipolar couplings. However, natural Mt, conventionally used as host matrix for the preparation of organoclays based on surfactants contains Fe (III) species in significant amounts, which induce strong electron-nucleus dipolar interaction, thus limiting the application of advanced experiments for the determination of the spatial proximity at the organo-mineral interface but also the arrangement of the intercalated aggregates.[5] Thus, research interests turned toward the use of equivalent host synthetic matrices as laponite, a hectorite, or saponite.[21-25] In the past years, hydrothermal synthesis allowed researchers to obtain Mt without any paramagnetic or ferromagnetic species (FeO and $Fe_2O_3$) in its composition while showing similar properties to their natural analogues.[33]

Thus, this study aims at (i) confirming the importance of the surfactant state in bulk solution in the surfactant aggregates onto the latter synthetic Mt with the comparison both its adsorption isotherm and X-ray diffraction patterns to those obtained with a natural Mt; (ii) characterizing at molecular and nanometer scales the surfactant arrangement and dynamics with respect to Mt surface by [1]H-^{13}C correlation (indirect detection ^{1}H INEPT), CP-MAS ^{13}C {^{1}H} NMR and high resolution [27]Al {[1]H} CP-[1]H-^{1}H spin diffusion experiments; and (iii) determining the main driving force between H-bonds, ion-dipole and Van der Waals interactions modulated through inorganic $Na^+$ exchangeable cations, leading to the adsorption of $C_{10}E_3$ onto the clay surface.

# Experimental Section

## Samples

The synthetic Na-exchanged montmorillonite (Na-S-Mt) was prepared as described in ref [33] (although a different nomenclature is used here). The formula obtained by a combination of an Inductively Coupled Plasma Optical Emission Spectrometry (ICP-OES) analysis using a Jobin-Yvon Ultima spectrometer and electron microprobe analyses of the solid clay mineral is $(Na_{0.68}Mg_{0.03})$ $(Al_{3.35}Mg_{0.65})(Si_{7.91}Al_{0.09})O_{20}(OH)_4$. This synthetic Mt exhibits analogous properties as natural clay mineral with a cation exchange capacity (CEC) of about 83 meq/100g and a specific surface area, determined with the adsorption of ethylene glycol, of 760 $m^2.g^{-1}$. Tri-ethylene glycol mono n-decyl ether $(C_{10}E_3)$ nonionic surfactant, purchased from Nikko Chemicals, Inc., (Tokyo, Japan), and assumed to have a purity > 99.8% was used without further purification. In aqueous solution, a lamellar $(L_\alpha)$ phase exists at room temperature with a $C_{10}E_3$ bilayer thickness close to 27.6 Å. [18, 34]

## Preparation of the $C_{10}E_3$ / clay organoclays (OC)

Several aqueous solutions of $C_{10}E_3$ were prepared at room temperature on a wide range of concentrations varying from $2.8.10^{-4}$ to $3.3.10^{-2}$ mol.$L^{-1}$ below and beyond the critical micelle concentration (*cmc*) which was previously estimated at $6.10^{-4}$ mol.$L^{-1}$. This compares with a prediction of $7.4.10^{-4}$ mol.$L^{-1}$ based on the length of the hydrocarbon chains and the number of ethylene oxide groups.[35] Below the concentration of $7.5.10^{-4}$ mol.$L^{-1}$, estimated as the experimental *cmc* in this work, the $C_{10}E_3$-water system appeared as an aqueous solution in monomers form, whereas above it, the surfactant self-assembles in a lamellar phase $(L_\alpha)$ which was checked by phase contrast optical microscopy.[34] The solutions were homogenized by stirring at room temperature for several days. $Na^+$-Mt in powder form was then dispersed into the surfactant solutions. The average pH value of the solutions was about $6.5 \pm 0.2$ and remained constant during the organoclay (OC) preparation. The obtained dispersions were then stirred for 24 h at 250 rpm. The OC samples, separated by centrifugation, were rinsed by water and dried at 90°C for 48 hours that expelled a large amount of water molecules from the hybrid materials, which may reorganize the surfactant aggregates. Nevertheless, previous thermal characterizations on the resulting dried OC revealed the presence of small amount of water (less than 3 % in weight) [16] and was attributed to adsorbed water onto external surface of OC which does not perturb the surfactant organization. Further works on the influence of the drying process needs to be undertaken and remains an open and difficult question and will be published elsewhere with the investigation of the adsorption and organization of several non-ionic $C_nE_m$ surfactants onto clay minerals in solution. The resulting OC were crushed using an agate mortar and we assumed that the water content could be neglected since it us under 3% in weight for the whole samples.

## Adsorption isotherm

The concentration of carbon in solution were measured using an element analyzer (Shimadzu TOC 5050 /SSM 5000-A) and were carried out at the 'Service central de mirco-analyse du CNRS' at Solaize in France. The amounts of adsorbed surfactant and equilibrium isotherm were determined on the basis of the concentration decrease after clay mineral impregnation.

## X-Ray diffraction (XRD)

The $d_{001}$ spacing's of the resulting OC were determined by the first *00l* reflection from the X-rays patterns which were recorded in a conventional θ-θ Bragg-Brentano configuration (Ni-filtered $CuK_{\alpha1,2}$ = 1.5418 Å) by using a model D8 Advance Bruker-AXS Powder X-ray diffractometer coupled with a linear Vantec-1 detector. The diffractograms were performed between 1 and 62° (2θ) with angular and time steps of 0.0328° and 1s respectively with the heating of the OC samples at 80°C. However, XRD patterns of samples heated at 80°C and those characterized at room temperature did not reveal any particular differences. A beam stop and a slit of variable divergence were used and the active area of the detector was limited as much as possible in order to reduce the scattering background at low angle.

## Nuclear Magnetic Resonance (NMR)

Prior NMR characterizations, the samples were dried again at 105°C during 24 hours. Then, the samples were introduced in the appropriate rotors in a glove box with a particular care to avoid any hydration of the OC. However, if hydration occurred, the amount of water may be negligible as X-ray diffraction data and previous thermal analyses revealed where adsorbed water was only located onto external surface of OC platelets. Moreover, the used of magic angle spinning (MAS) NMR methods may favor dehydration of adsorbed molecules and ensure to mainly work onto dehydrated samples for the characterization of surfactant aggregates.

Solid-state NMR experiments were conducted at room temperature (i.e. 21°C, controlled by an air conditioning system) at 17.6 T, corresponding to $^1$H, $^{13}$C, and $^{27}$Al Larmor frequencies of 750.1, 188.6, and 195.5 MHz, respectively, on Bruker AVANCE III 750 spectrometer. All $^1$H, $^{13}$C chemical shifts are given relative to (neat) TMS at 0 ppm.

$^{13}$C NMR data were collected with a 4 mm double resonance probehead at a MAS frequency of 13 kHz. The quantitative $^{13}$C MAS NMR spectrum was collected with a recycling delay of 120 s, and 512 scans for signal averaging. The $^{13}$C{$^1$H} CP-MAS spectrum was acquired with a contact time of 250 μs, with 4096 transients. The $^{13}$C{$^1$H} refocused INEPT experiment used coherence transfer and refocusing echoes of 1.538 ms (20 rotor periods. All $^{13}$C NMR experiments, including the two-dimensional experiments described below, used heteronuclear $^1$H decoupling at a nutation frequency of 70 kHz with SPINAL64.

The two-dimensional (2D) $^{13}$C{$^1$H} HETeronuclear CORrelation (HETCOR) experiment used a CP contact time of 500 μs, and 192 transients per $t_1$ increment with a recycling delay of 2.5 s. The indirect dimension was collected with 128 increments with frequency-switch-Lee-Golburg (FSLG) homonuclear $^1$H-$^1$H decoupling [36] at a nutation frequency of 70 kHz, which led to a scaling factor of 0.50 (measured from a homonuclear $^1$H-$^1$H experiment conducted with the same decoupling conditions in the indirect dimension). Total experimental time was 17h. The 2D refocused Insensitive Nuclei Enhanced by Polarization Transfer (INEPT) experiment [37] used coherence transfer and refocusing echoes of 1.538 ms (20 rotor periods), 128 transients with a recycling delay of 2s, and 128 increments in the indirect dimension (total experimental time: 19h). Decoupling of heteronuclear $^1J_{CH}$ scalar couplings in the indirect $^1$H dimension was achieved with a refocusing 180° pulse in the center of the evolution period.

The 2D $^{13}$C-$^{13}$C refocused INcredible Natural Abundance DoublE Quantum Experiment (INADEQUATE)[38, 39] was conducted on neat $C_{10}E_3$ (a viscous liquid at room temperature) at 9.4 T, using a solid-state 4 mm probehead with a slow MAS frequency of 800 Hz and low-power (2 kHz) decoupling on the $^1$H channel to suppress the effect of $^1J_{CH}$ scalar couplings. Both echo durations were set to 7 ms. 1536 scans were used for signal averaging, with 196 increments for the indirect dimension and a recycle delay of 0.15 s (total experimental time: 13 h).

All $^1$H and $^1$H{$^{27}$Al} NMR experiments were collected with a 1.3 mm double resonance probehead at MAS frequencies between 60 and 64 kHz. Quantitative spectra are obtained from $^1$H echo-MAS experiments with short echo duration of 8 rotor periods (125 μs) to ensure complete elimination of background signals, with a total of 16 scans and a recycling delay of 10 s. The experiment combining $^1$H{$^{27}$Al} cross-polarization and $^1$H-$^1$H spin-diffusion used a $^{27}$Al -> $^1$H cross-polarization time of 1 ms and spin-diffusion mixing times of between 15 μs and 500 ms. Signal was averaged over between 512 and 3084 scans.

The modeling of $^{13}$C and $^1$H NMR spectra used a home-made Matlab program designed to fit simultaneously a series of one-dimensional datasets recorded in different conditions with a single set of lineshape parameters (position, width, Gaussian-Lorentzian ratio) and different amplitudes. This procedure increases considerably the reliability of the models when strong overlaps between peaks are observed.

# Results and Discussion

## Importance of a surfactant state in an aggregation process

   The equilibrium adsorption isotherm represents one important data to understand the mechanisms of adsorption of fluids onto solid surfaces. The adsorption of $C_{10}E_3$ was performed on a wide range of concentrations, below *cmc* with surfactant in monomer and above it in a lamellar phase. As previously observed in a natural Mt, below a concentration of $7.5.10^{-4}$ mol.L$^{-1}$, $C_{10}E_3$ monomers cover the Mt surface, revealing the strong affinity between $C_{10}E_3$ and the phyllosilicate layers. Above the *cmc* $C_{10}E_3$ self-assembles in a lamellar phase, the lineshape of the adsorption isotherm similarly evolves as that of a natural Mt (in dashed line) with a continuous growth of the adsorbed amount as the equilibrium concentration is increased (Fig. 1a). While the Langmuir equation was successfully applied for modeling the adsorption of surfactant on Mt surface as previously described in refs[35,36], this does not ensure Langmuir model assumptions are fulfilled here. Indeed, this model assumes the adsorption occurs on homogenous Mt sites with a constant adsorption force between surfactant/adsorbent.[10, 40, 41] The formation of L$\alpha$ induces a change of adsorption mechanism and may explain why the adsorption isotherm could not be fitted properly by a Langmuir adsorption model here. Nevertheless, while the adsorption of $C_{10}E_3$ cannot be entirely fitted on the whole concentration range, we used the linear form of the Langmuir model to separately monitor both monomer and a lamellar phase regimes (Fig. 1b). The linear form of the Langmuir isotherm model is written by the following equation:[42]

$$\frac{1}{q_e} = \frac{1}{q_{max}} + \left(\frac{1}{q_{max}K_L}\right)\frac{1}{C_e}$$

where $q_e$ is the $C_{10}E_3$ equilibrium adsorbed amount on Mt (mol.g$^{-1}$), $C_e$ the $C_{10}E_3$ equilibrium concentration in the resulting solution (mol.L$^{-1}$), $q_{max}$ the maximum adsorption capacity of the Mt (mol.g$^{-1}$) and $K_L$ is the Langmuir adsorption constant (L.mol$^{-1}$) and is related to the free energy ($\Delta G°$) of adsorption by the relation:

$$\Delta G° = -RT \ln K_L$$

   Plots of $\frac{1}{q_e}$ as a function of $\frac{1}{C_e}$ in both regimes give two distinct straight lines, leading to $K_L$ constants close to 8175 and 16000 L.mol$^{-1}$ and standard free energies $\Delta G°$ of -21.9 and -24.2 kJ.mol$^{-1}$ for $C_{10}E_3$ adsorbed as monomers and in the L$\alpha$ phase, respectively. This suggests, despite a small difference in $\Delta G°$ between the two regimes, that the adsorption was rapid and more spontaneous in L$\alpha$, with the aggregation of $C_{10}E_3$ in membranes (i.e. bilayer arrangement). The adsorption in L$\alpha$ involves a cooperative process stacking the $C_{10}E_3$ in bilayers on the Mt surface (i.e. homeotropic anchoring) whereas in monomer regime, $C_{10}E_3$ covers the accessible clay surface with a planar anchoring. The amounts of adsorbed surfactant $q_{max}$ estimated from Langmuir fitting procedure are $5.8.10^{-4}$ and $1.3.10^{-3}$ mol.g$^{-1}$ in monomers and in the lamellar phase respectively. With an apparent packing area of 0.76 nm$^2$,[18] the maximum amount of $C_{10}E_3$ adsorbed in a lamellar phase does not appear to entirely the whole accessible surface of the synthetic clay Mt that is 10% smaller to that of the natural Mt ($q_m$=1.6 x $10^{-3}$ mol.g$^{-1}$). Both natural and synthetic montmorillonite show a heterogeneous surface, with nevertheless the presence of much more defects in the case of a natural Mt comparatively to Na-S-Mt. This latter point combined to well-crystalline particles may be a possible explanation for the low (by 15%) $C_{10}E_3$ maximum adsorption value.[33]

   The inter-layer organization of the organoclay composites obtained at various $C_{10}E_3$ concentrations is shown in Figure 2 by the positions of the small-angle XRD basal (00*l*) reflections. As expected, the *d$_{001}$* basal spacings for the concentration range in which $C_{10}E_3$ self-assembles in L$\alpha$ is about 37.2 Å (sample # 3 [$C_{10}E_3$] = $7.5\times10^{-3}$ mol.L$^{-1}$), confirming the proper intercalation of a bilayer within the interlayer space of the synthetic Mt (Fig. 2a,b).[18] Moreover, the ordering within the silicate layers is particularly enhanced at large $C_{10}E_3$ concentrations, as manifested by several *00l* reflections, which are not observed

concentrations in monomers regime. Below the *cmc*, the evolution of the $d_{001}$ spacings as a function of the equilibrium $C_{10}E_3$ concentration show two distinct steps at about 13.5 (sample # 1 [$C_{10}E_3$] = $5\times10^{-4}$ mol.L$^{-1}$) and 17.7 Å (sample # 2 [$C_{10}E_3$] = $2\times10^{-3}$ mol.L$^{-1}$) pointing out the intercalation of a lateral monolayer and lateral bilayers respectively, based on the height of thickness of bilayer size of $C_{10}E_3$. These $C_{10}E_3$ aggregates arrangements at concentrations up to 9.2 x $10^{-4}$ mol.L$^{-1}$ are consistent to those observed with natural Mt. However, with the use of a synthetic Mt, the reorganization in a tilted bilayer with a full extension of the alkyl chains was not observed. Such surfactant aggregates expand the interlayer space to about 43 Å in a natural Mt.[16,18] Here, the mass transfer with the increase of concentration of surfactant, combined to small-scale particle were not sufficient to favor such a stretched bilayer organization within the interlayer space.[16]

**Structure and dynamics of the $C_{10}E_3$ aggregates**

  While results obtained by both X-Ray diffractions patterns and adsorption isotherms at equilibrium support the aggregation of $C_{10}E_3$ in a bilayer arrangement (at high $C_{10}E_3$ concentration) and reveal structural changes of the Na-S-Mt organoclays as the concentration of $C_{10}E_3$ varies, they do not provide any clear insights onto the molecular structure and conformation of the intercalated surfactant. In order to probe both the structure and the dynamics of the surfactant aggregates confined within the interlayer space of Mt, we used solid state NMR on dehydrated organoclay (OC) samples exhibiting three distinct structures identified by X-ray diffraction results (Figure 2).

  Solid-state $^{13}$C NMR spectra of organoclay samples prepared at different concentrations of $C_{10}E_3$ feature a number of distinct of peaks corresponding to different parts and fractions of the intercalated surfactant molecules. Figure 3a-c shows the quantitative $^{13}$C NMR spectra collected for organoclay samples prepared with $C_{10}E_3$ concentrations of $5\times10^{-4}$, $2\times10^{-3}$, and $7.5\times10^{-3}$ mol.L$^{-1}$, labeled as samples # 1, 2 and 3 respectively, which are characterized respectively by basal distances of 13.5, 17.7, and 37.2 Å. To analyze these differences in detail, however, it is necessary to first assign all $^{13}$C NMR signals to the corresponding parts of the surfactant chains. This step was performed by comparisons with a spectrum collected for the pure surfactant, which is a viscous liquid at room temperature. The spectrum shown in Figure 3d, is a refocused INADEQUATE ("INcredible NAtural Abundance Double QUAnTum Experiment") [38, 39] which shows pairs of correlation peaks for pairs of $^{13}$C nuclei connected by a direct C-C bond, which appear at both individual frequencies in the horizontal dimension, and at the sum of these frequencies in the vertical (double-quantum) dimension. This makes it possible in principle to identify the different systems of connected C carbons in the surfactant molecule, albeit with some limitations. First, the experiment suffers from sensitivity issues associated with the low probability to find $^{13}$C-$^{13}$C pairs given the natural abundance of this isotope (ca. 1%). This explains why no signal could be observed for the terminal CH$_3$ despite a rather long experimental time. Moreover, correlations between peaks of identical frequencies cannot be observed because the effect of the scalar coupling between them vanishes in this case. Despite these limitations, it was possible from this spectrum and the relative intensities of the peaks in the quantitative 1D spectrum (shown on top of the 2D spectrum) as well as with the work of Ferreira et al. [43] to unambiguously identify all of the individual signals in liquid $C_{10}E_3$, and by comparison, in surfactant molecules intercalated in the clay samples (Fig. 3a-c). Interestingly, many distinct fractions of the surfactant show completely (as in Fig. 3c) or partially (as in Fig. 3a) resolved $^{13}$C NMR signals, which means that these contributions can be analyzed individually. The hydrophilic headgroup (between 60 and 75 ppm) and hydrophobic tail (between 14 and 35 ppm), in particular, are perfectly well separated, and it is also possible to distinguish among these the end-chain carbons (C1 and C15-16, respectively), even for sample # 1 showing the broadest lines ([$C_{10}E_3$] = $5\times10^{-4}$ mol.L$^{-1}$, Fig. 3a).

  The $^{13}$C NMR spectra indeed show extremely pronounced differences in peak widths as a function of the surfactant concentration used for the synthesis, which indicates dramatic differences in the extents of structural disorder and/or dynamics of the intercalated molecules. These differences point in turn to different modes and strengths of interactions between the surfactant molecules and the clay layer surfaces.

At high surfactant concentrations (Fig. 3c), the $^{13}$C spectrum looks remarkably similar to the spectrum of pure $C_{10}E_3$, which indicates that chains are extremely mobile and the corresponding signals entirely averaged out on the timescale of the NMR experiment (frequencies on the GHz range or higher). Only the terminal signals C1 (at 62 ppm) and C2 (at 73 ppm) of the hydrophilic headgroups are somewhat broadened, indicating that these sites interact more strongly with the surface. This observation is fully compatible with the large basal spacing measured by XRD for this sample (37.2 Å). As the surfactant concentration decreases, the intensities of the narrow "liquid-like" signals decrease substantially in favor of considerably broader signals indicating chemically-disordered species. Such chemical disorder arises from distributions of chain conformations and/or inter-chain interactions among surfactant molecules that are either immobilized or with motions too slow to be averaged out on the time scale of the NMR experiment (significantly lower than ca. $10^8$ or $10^7$ Hz).

The analyzes of these surfactant motions can be deepened by quantifying the relative amounts of rigid and mobile fractions of the $^{13}$C NMR signals assigned to the various parts of the surfactant molecules. Differences of mobility may indeed be observed not only among samples, but also within each sample, where they can be exploited to generate spectral contrast between the mobile and rigid fractions of surfactant located in the interlayer space of the clay mineral. This is illustrated in Figure 4 by a series of three spectra collected for sample # 2 ($[C_{10}E_3] = 2\times10^{-3}$ mol.L$^{-1}$) with three distinct NMR pulse sequences that are affected in different ways by molecular motions. This approach has been introduced by Topgaard and co-workers for the characterization of the structure and dynamics of surfactant molecules in mesoporous silica, and named "$^{13}$C Polarization Transfer solid state NMR ($^{13}$C PT ssNMR)" [44, 45]. The first spectrum (Fig. 4a) is the quantitative $^{13}$C NMR spectrum (same as in Figure 3b), in which the signal intensity reflects the relative site populations, independent on the molecular motion. The second experiment (Figure 4b), called refocused INEPT ("Insensitive Nuclei Enhanced by Polarization Transfer"), is classically used in liquid-state NMR to identify $^{13}$C signals connected to $^1$H nuclei, as in CH$_2$ or CH$_3$ groups, for example. This experiment does not work for rigid solids because, even under fast MAS, the strong dipole-dipole interactions between $^1$H and $^{13}$C nuclei cause rapid dephasing of the signal during the sequence. In the context of the confined surfactant molecules studied here, this experiment selectively reveals the sharp $^{13}$C signals due to fractions of surfactants with fast (liquid-like) dynamics that average out the $^{13}$C-$^1$H dipolar interactions. The third experiment (Figure 4c) does the opposite and instead selectively emphasizes $^{13}$C NMR signals from rigid surfactant fractions. This experiment is a classical $^{13}$C{$^1$H} CP-MAS experiment, recorded in this case with a very short cross-polarization contact time (50 μs) to transfer magnetization from $^1$H nuclei to nearby $^{13}$C nuclei for detection. Contrarily to the INEPT experiment, the CP-MAS experiment works only for solids, and not for liquids. At short contact times, the magnetization transfer will only occur for fractions characterized with strong $^{13}$C-$^1$H dipolar interactions, *i.e.*, that are not averaged out by molecular motions.

Such a combination of spectra emphasizing either the rigid or the mobile parts can be used to derive a unique set of peaks (defined as pseudo-Voigts) described by their position, full width at half maximum (FWHM) and Gaussian to Lorentzian ratio, that is able to model all three spectra. This procedure is achieved by adjusting a single model containing all necessary peaks to all three spectra at the same time, allowing only the intensity of each peak to vary from one spectrum to the other. The best models obtained with this procedure, shown in red on top of each experimental spectrum in Figure 4 with the individual components shown underneath in grey, accurately reproduce all three spectra. Such a simultaneous fit of several strongly-contrasted spectra with a single model results gives a high level of confidence on the decomposition on the (most challenging) quantitative spectra, where the overlap of broad and narrow resonances could otherwise cause strong uncertainties, especially in the crowded regions between 20 and 40 ppm and between 65 and 80 ppm. This is turns provides accurate quantifications of the relative amounts of mobile and rigid fractions for all fragments of the intercalated surfactant molecules.

Spatially-resolved rigid/mobile repartitions along the surfactant chains confirm the inter-layer organization hypothesized based on the basal distances derived from XRD data and provide further details onto the way the surfactants interact with the clay surface. X-ray diffraction data support the confinement of $C_{10}E_3$ in the internal structure of the clay mineral. If the internal surface of clay mineral is accessible (i.e. the interlayer space which is this case with the intercalation of the nonionic surfactant), its contribution represents about 95% of the whole surface area of the clay mineral (about 760 $m^2.g^{-1}$ determined with ethylene glycol adsorption) giving thus a minor role to the contribution of the surfactant adsorbed onto the external surface of the clay platelets. Without being confined, these adsorbed $C_{10}E_3$ molecules appear extremely mobile or display a fast dynamics in the NMR time scale window. While it is rather hard to exclude their small contribution in the NMR signal, the Figure 5(a-c) shows the relative proportions of mobile and rigid surfactant fractions confined within the interlayer space of the synthetic clay mineral represented for each sample with the different parts of the surfactant molecules ordered as along the chain, from the hydrophilic terminal alcohol group (C1) to the hydrophobic terminal methyl group (C16). At smallest surfactant concentrations ([$C_{10}E_3$] = $5\times10^{-4}$ mol.L$^{-1}$, Fig. 5a) both components assigned to the surfactant headgroup (C1 and C2-7) are purely rigid (lower than ca. $10^8$ or $10^7$ Hz) with no detectable mobile fraction, indicating as expected a strong confinement effect within the interlayer space of the host matrix that slow down the dynamics of $C_{10}E_3$, which was observed for the whole NMR pulse sequences. This extreme rigidity of the surfactant headgroups probably result to their close interaction between the hydrophilic groups and Mt surface. While the rigid fraction also strongly dominates for other parts of the surfactant chains, mobile fractions are nevertheless detectable and most intense for the end-chain carbons C14-C16. Given the basal distance of 13.5 Å measured for this sample and a clay layer thickness of 7 Å, there seems to be enough room to cover both the top and bottom clay surfaces with surfactant molecules, and preferentially their mobile fractions. If the surfactant concentration is not too high, one may imagine that there may be a few scarce spaces within this two-layer surface decoration for some parts of the hydrophobic fragments, and especially those of the end of the chains to remain mobile. With a picture of headgroups in close interaction with Mt surface, $C_{10}E_3$ alkyl chains occupy the middle of the interlayer space and thus are less affected by the effects of Mt surface impacting their mobility. Szczerba et al. [46] have used molecular dynamics to study smectite – ethylene glycol composites, using the CLAYFF force field, [47] whose ability to accurately predict the structure and dynamics of clays and their intercalated water and cations is well established. [48, 49] Their calculations show that on these systems (which are hydrated in contrast to ours which are dehydrated) basal spacings of the order of 16 to 17 Å accommodate in every case two well-separated layers of ethylene glycol (at least as far as C atoms are concerned) with Na$^+$ ions located primarily at the center. The slightly smaller basal spacing observed here (which may be explained by a dehydrated state)[16] seems nevertheless compatible with a similar organization, and in any case too large to have only a single layer of ethylene glycol monomers decorating the surface, which would leave much empty space.

At higher surfactant concentrations (sample # 2 [$C_{10}E_3$] = $2\times10^{-3}$ mol.L$^{-1}$, Fig. 6b) the hydrophilic fragments of the surfactant molecules are still largely immobilized, with only ca 5% of the C2-7 fragments measured as mobile, but ca. 30% of the hydrophobic tails now exhibit a liquid-like behavior. With a measured basal distance of 17.7 Å, slightly larger than those simulated for the ethylene glycol - water – Mt complexes, one can imagine that the decoration of the top and bottom clay surfaces by $C_{10}E_3$ now leaves enough space for some of the tail CH$_2$ and CH$_3$ fragment forming something that may be seen as a third layer of carbon atoms at the center of the inter-layer space. This basal distance of our dehydrated $C_{10}E_3$-Mt organoclay sample is nevertheless considerably smaller than the value of 24 Å simulated by Krishnan et al. for a hydrated poly-ethylene glycol (PEG) – Mt complex, and in which a four-PEG-layer organization was observed. [50]

A marked increase of the amount of mobile fractions is observed for highest surfactant concentrations (sample # 3 [$C_{10}E_3$] = $7.5\times10^{-3}$ mol.L$^{-1}$, Fig. 5c), consistent with the vertical orientation of surfactant chains hypothesized by the sudden increase of basal spacing (from 1.77 to 3.72 nm between $2.0\times10^{-3}$ and

$3.0\times10^{-3}$ mol.L$^{-1}$, see Figure 2). While highest for end-hydrophobic-chain regions (ca. 80%), the fraction of mobile groups is nevertheless high also for the hydrophilic domains (C2-C7) with less than 40% of rigid carbon sites detected. The observed mobile fraction for C15 shows nevertheless a slower dynamics than for the adjacent carbons C14 and C16, an experimental small difference within the error bars (confidence interval of 95%), estimated from the data deviation of the fitting procedure. Only the terminal hydrophilic carbon C1 in this case is largely rigid (and therefore giving no detectable signal in the refocused INEPT experiment). These results consequently suggest that in this composite, the surfactant molecules interact with the clay surface essentially through their terminal OH group, no more than 3% of which may be considered mobile. The closest carbons (C2, C3…) have their mobility reduced as a result, but the rest of the chain is dominated by a liquid-like behavior consistent with their location within the interior of the vertical surfactant bi-layer, where they are only subject to weaker inter-chain Van der Waals interactions. A possible explanation for the small fraction of hydrophobic chains that remain rigid in this composite is that there may still be a small number of interlayer spacings that have not yet expanded to accommodate a vertical bi-layer, and where the surfactants adopt instead the lateral two-layer organization observed for lower C$_{10}$E$_3$ concentrations between $9.0\times10^{-4}$ and $2.0\times10^{-3}$ mol.L$^{-1}$ (e.g., as in sample # 2). Quantitative $^{13}$C NMR data hence sheds light on how the organization of the surfactant molecules and mobilities of the different sections of the surfactant chains correlate with the inter-layer spacing measured by diffraction.

The location of the different fractions of the surfactants within the inter-layer space can in principle be established from NMR data, by exploiting the exchange of magnetization that can be triggered between the different NMR-active nuclei present in the system. Such magnetization exchange can occur directly through the dipolar coupling between two nuclei (as between $^1$H and $^{13}$C nuclei in the CP experiment of Figure 4c) or through more complicated spin-diffusion processes involving multiple couplings between abundant nuclei of the same type (typically $^1$H). In the organoclay composites studied here, the location of surfactant moieties could be qualitatively established by means of magnetization transfers between the $^{27}$Al nuclei of the clay and the protons of the intercalated surfactant molecules. A prerequisite, however, is to evaluate the resolution that can be obtained on these systems with $^1$H NMR, since this is often a strongly limiting factor. The dense network of dipolar couplings between abundant protons with large gyromagnetic ratios indeed generally causes severe broadening of $^1$H NMR lines even under fast MAS conditions. The combination of high magnetic fields, which increase the separation between peaks (expressed in frequency units), and the very fast MAS rates available nowadays (up to 110 kHz), which reduce the residual dipolar broadening, provides favorable conditions.

Two-dimensional $^{13}$C-$^1$H correlation experiments are used to distinguish and assign the $^1$H NMR signatures of the different regions of the surfactant molecules. Figure 6 shows a superposition of two such spectra collected for samples with low and high concentrations of C$_{10}$E$_3$, with the $^{13}$C dimension in the horizontal axis and the $^1$H dimension in the vertical axis. The blue spectrum was recorded for sample # 1 ([C$_{10}$E$_3$] = $5\times10^{-4}$ mol.L$^{-1}$) with a solid-state-type experiment probing spatial proximities between $^1$H and $^{13}$C nuclei (the two-dimensional equivalent of the CP experiment of Figure 4c). Correlation peaks in this spectrum preferentially point to CH bonds (associated with short C-H distances and hence strong dipolar couplings) and allow us to relate the distinct $^1$H NMR signals to the corresponding attached carbon. Hence, the $^1$H peak at 3.8 ppm on the $^1$H NMR spectrum (shown on the right side of the 2D spectrum) corresponds to protons attached to O-CH$_2$ carbons C1-C7 of the hydrophilic region. Similarly, the $^1$H peaks at ca. 1.4 and 1.0 ppm correspond respectively to CH$_2$ protons attached to groups C8-C15 of the hydrophilic chain and to CH$_3$ protons of the terminal C16 group. Other features of the $^1$H NMR spectrum, such as the broad shoulder centered at 2.2 ppm correspond to clay hydroxyl groups connected to two Al atoms in the octahedral layer (Al$_2$OH groups).[5] Another peak is expected around 1 ppm due to clay hydroxyl groups connected to one Al and one Mg atom (MgAlOH groups) but it is hidden by the surfactant signals.

The red spectrum in figure 6b, collected on sample # 3 ([$C_{10}E_3$] = $7.5 \times 10^{-3}$ mol.L$^{-1}$), is a liquid-state-type experiment probing the existence of through-bond couplings between $^1$H and $^{13}$C nuclei, and corresponds to the two-dimensional equivalent of the INEPT experiment of Figure 4b. Correlation peaks are observed at similar positions as in the dipolar-mediated experiment discussed above (in blue), but considerably narrower because this experiment selectively probes the mobile fractions of the surfactant present in large proportions in this sample. Despite these considerably narrower lines, however, the resolution in the $^1$H dimension is substantially lower than in the $^{13}$C dimension since the individual signals other than the C1-C7, C8-C15 and C16 groups cannot be clearly separated. These three distinct groups of $^1$H signals are nevertheless sufficient to perform some qualitative analyses of the surfactant organization in the inter-layer space.

An NMR sequence of radio-frequency (RF) pulses was specifically designed to probe the proximities between $^1$H signals of the surfactant molecules and the clay. This sequence, depicted in Figure 7a, contains 2 steps identified with circled numbers. The first one is an excitation of $^{27}$Al nuclei of the clay followed by a double irradiation of $^{27}$Al and $^1$H nuclei to achieve a magnetization transfer from the former to the latter (symbolized by the green arrow in Fig. 7a and 7b) through $^1$H-$^{27}$Al dipolar couplings by the cross-polarization mechanism. This step is expected to build $^1$H magnetization selectively on the clay hydroxyl groups, which are strongly bound (via apical O atoms) to the clay Al atoms (see examples in refs [5, 31]), as depicted by the green arrow in the schematic of Figure 7b. The second step starts with a storage of the $^1$H magnetization hence created along the $^1$H magnetic field, followed by a propagation of this magnetization among nearby protons by the spin diffusion process between multiply-coupled spins, symbolized with the orange arrow in Fig. 7a and the orange halo in Fig. 7b). The resulting magnetization is finally excited again for detection of $^1$H signals to which propagation occurred, and in particular the surfactant $^1$H nuclei in the organoclays studied here. The second step of this pulse sequence is directly inspired from experiments designed to probe the interactions between templating agents (e.g. tri-block co-polymers or alkylammonium surfactants) and silica (or siloxane) surfaces.[51] [52]

Although molecular dynamics may average dipolar coupling leading to slower rates of transfer at an equivalent distance, what is expected from the experiment described above is to observe different rates of transfer to $^1$H nuclei located within different fractions of the incorporated molecules, to then estimate their relative proximities to the clay sheets (as represented by their OH groups). Figure 7d shows the $^1$H echo-MAS spectrum collected for sample # 2 prepared with intermediate $C_{10}E_3$ concentration ($2 \times 10^{-3}$ mol.L$^{-1}$), and Figure 7e a series of experiments collected for the same sample with the pulse sequence described above, using different $^1$H-$^1$H spin-diffusion mixing times. When the mixing duration is too small to allow diffusion of the magnetization among $^1$H nuclei (Figure 7e, bottom), only the signals characteristic of the clay OH groups (since the samples are dehydrated) are detected because they are bonded via basal O atoms to $^{27}$Al nuclei. Signals at 2.1 and 1.8 ppm correspond to Al$_2$OH and MgOH moieties, respectively, as demonstrated in ref. [5] for "as-made" synthetic Na-montmorillonite (sample whose XRD data are shown in black in Figure 2). With increasing mixing times other signals appear: first the -CH$_2$-O- signals characteristic of the surfactant headgroup, and very shortly after this the alkyl CH$_2$ and even CH$_3$ signals of the hydrophobic tail, consistent with the lateral orientation of the surfactant chains hypothesized for this sample.

Comparisons of the growth rates of the $^1$H NMR signals as a function of the $^1$H-$^1$H spin-diffusion mixing time for different samples confirm the structural and dynamic information established from XRD and $^{13}$C NMR data. Figure 8a,c,e shows the decomposition of quantitative $^1$H NMR spectra obtained for each sample using a multiple-spectrum fitting procedure to increase the confidence in the fits, as for $^{13}$C data. This approach is particularly critical here given the strong overlap between clay and surfactant $^1$H NMR signals. The positions, widths and shapes of the former, shown in grey in Figure 8a, c and e, are nevertheless confidently established using $^{27}$Al-edited spectra (not shown) that selectively reveal these signals on the basis of their proximity with clay Al sites (as in the bottom spectrum of Figure 7e), which

greatly facilitates the modeling of the others. These individual components are then used to fit all series of $^1$H-$^1$H spin-diffusion experiments (allowing only the amplitudes to vary).

   This makes it possible to track the evolution of a number of $^1$H signals as a function of the $^1$H-$^1$H spin-diffusion mixing time for all samples. The results, shown in Figure 8b, d, and f reveal nearly identical transfer rates for all samples to rigid fractions of the surfactant molecules, whether they are located in the hydrophilic headgroup (in red) or in the hydrophobic tail (in purple). Hence, while the fractions of these rigid moieties decrease systematically with increasing basal distances, indicating that surfactant chains spend less time in this "rigidified" state, the strength of their interactions with the clay surface does not decrease. This suggests that the interaction mechanism remains the same despite different inter-layer arrangements when the surfactant concentration varies. In contrast, the mobile fractions of both the headgroup (in orange) and the tail (in blue) show strong differences between samples, with transfer rates that increase systematically with the basal distance. This is another manifestation of the gradual verticalization of the surfactant chains, which is associated with a higher extent of mobility of the increasingly large fractions of chain fragments that do not interact with the clay and are not constrained by the proximity to rigid groups on the same molecule.

**Ion dipole interaction as the main driving force in the adsorption**

   The mechanism(s) that dominate the interactions between the rigid fractions of the surfactant molecules may now be examined in light of $^{23}$Na data collected for samples with and without surfactant molecules intercalated in their inter-layer galleries, in both as-made and dehydrated forms to reveal the role played by water molecules. For this purpose, in contrast to previous experiments where the organoclays samples where exclusively dehydrated (or hydrated at a rate below 3% in weight) in order to probe the surfactant aggregates. For $^{23}$Na experiments, the samples, including synthetic Mt and organoclays, were dehydrated with a process explained in the experimental section, and hydrated in ambient conditions (room temperature and hygrometry of 60%) for one week. The hydration was confirmed by X-Ray diffraction experiments, which showed a $d_{001}$ spacing of the synthetic Mt at a value close to 12.5 Å, underlining the solvation of the Na$^+$ cations by one water layer, while thermal analysis revealed an amount of water close to 4-6 % in weight for organoclay sample # 3 (XRD patterns did not show any difference in the $d_{001}$ spacing for both hydrated and dehydrated OC sample at high concentration). Figure 9a for instance shows the comparisons of $^{23}$Na NMR spectra collected for as-made and dehydrated Na-montmorillonite, in the absence of surfactant molecules. As it is well known in this case the mobility of Na$^+$ cations is considerably reduced in the dried form, both as a result of the loss of the cation hydration sphere and the strong confinement resulting from decreased inter-layer space.[9] This decreased mobility is manifested by the broadening and right-shift of the $^{23}$Na NMR line due to incomplete time-averaging of the second-order quadrupolar interaction, as has been discussed in detail by Okhubo *et al*.[9]. With surfactant molecules in the inter-layer space, in contrast, the effect of dehydration on the $^{23}$Na NMR lines is very limited (Fig. 9b), indicating that the Na$^+$ cations remain extremely mobile. This indicates that the amount of water in the organoclay is very small (4-6 % in weight as it was estimated through thermal analysis) and that Na$^+$ cations are most likely solvated in this case by the hydrophilic fractions of the surfactant molecules. In the four-PEG-layer arrangement predicted by Krishnan and coworkers for a PEG – Na-Mt composite with a basal spacing 24 Å,[50] Na$^+$ cations were found to be primarily located at the layer surface and between PEG-carbon layers 1-2 and 3-4, and to a lower extent in the center of the inter-layer domain (between carbon layers 2 and 3). In the C$_{10}$E$_3$ – Mt composites studied here, the presence of hydrophobic chains most likely results in the expulsion of Na$^+$ cations from the central inter-layer region. At low and intermediate surfactant concentrations, where both the surfactant headgroups and tails are lying parallel to the surface in one- (for c= 13.5 Å), two-, or three-layer (for c = 17.7 Å) arrangements, Na$^+$ cations most likely concentrate at the clay surface to avoid contact with the hydrophobic groups (whether mobile or rigid) and form ion-dipole interactions with the O atoms of the hydrophilic fragments. At higher concentration, where not only the hydrophobic tails but also significant fractions of the hydrophilic

headgroups adopt a vertical orientation, Na$^+$ cations can find O atoms to compensate their charge further away from the surface, and are consequently dispersed over a considerably larger domain than in the samples prepared with lower surfactant concentrations.

Solid-state $^1$H NMR data collected for the same series of samples (Figure 9c and d) shed light on the role played by hydrogen bonds in the interactions between the surfactant molecules and the clay surface. It is well known that the $^1$H chemical shifts of hydroxyl groups are strongly affected by hydrogen bonds to nearby proton acceptors [53, 54] (such as O atoms on oxide surfaces, see for example refs [31, 55, 56]). In ref. [5] we have shown that the $^1$H shifts of both types of clay OH sites in Na-Mt could be predicted accurately by DFT calculations conducted on models where H$_2$O molecules were omitted, *i.e.* with no H acceptor in the inter-layer space. This means that H bonds between the clay hydroxyl groups and water molecules are weak in as-made Na-Mt, a result that is confirmed by the absence of change in the positions of OH $^1$H NMR peaks when the sample is dehydrated (Fig. 9c). This minor role played by H bonds is also true in the organoclay, since the $^1$H NMR peak positions of the clay OH moieties are identical to the non-intercalated sample (see Al-edited spectrum at the bottom of Figure 8c). With H bonds playing such a minor role, and in the absence of positive charges in the surfactant headgroup, it seems that the interactions between the C$_{10}$E$_3$ molecules and the clay surface are primarily governed by ion-dipole interaction or/and Van der Waals forces. This is in agreement with the rather slight differences observed between the hydrophobic and the hydrophilic regions of the surfactant molecules (maybe with the exception of the hydrophilic end-chain) in terms of relative populations of mobile and rigid fractions, and with the similar dynamics of the rigid fractions, independent on the location along the surfactant chain.

## Conclusion

The aggregation of non-ionic surfactants resulting from their adsorption of aqueous solution to a solid surface is currently attracting considerable scientific interest due to their potential applications (detergency, flotation, oil recovery agents, water-based drilling fluids, and organoclays materials with the use of clay minerals). In contrast to cationic surfactants where the main driving force involves electrostatic interactions that disrupt any micelle adsorption, leading to irregular aggregates, the interaction of nonionic surfactants with layered surfaces results in a variety of distinct morphologies. The observed bilayers and spherical structures formed by nonionic surfactants are reminiscent to those observed for the bulk surfactant phases with nevertheless some different characteristics. In this study, C$_{10}$E$_3$ nonionic surfactant was successfully adsorbed and intercalated in a synthetic montmorillonite (Na-S-Mt), having no iron in its chemical composition, and obtained through a hydrothermal synthesis route. The surfactant aggregates within the interlayer space of Na-S-Mt showed similar organization to those obtained in an analogous natural clay mineral with a bilayer arrangement once C$_{10}$E$_3$ self-organized in a lamellar phase which can be studied in more detail through the measure of $^1$H-$^{13}$C residual dipolar couplings. [57] This latter observation confirmed the importance of a surfactant state in organoclay preparation and pointed out the universality of the aggregation of self-assembled membrane phases made of nonionic surfactant onto a clay mineral surface. A multi-nuclear investigation of three samples characteristics of the different of arrangements of the surfactant aggregates in a lateral monolayer, a lateral bilayer and a normal bilayer in the hybrid materials was conducted to understand at very fine level both their molecular structure and dynamics. Despite the confinement of the surfactant molecules in the inter-layer space of a clay mineral host material, the resolution of solid state $^{13}$C NMR spectra was sufficient to probe and precisely assign the entire moieties of C$_{10}$E$_3$ in the whole surfactant organizations. Quantitative $^{13}$C NMR measurements combined with $^1$H-$^{13}$C correlation experiments for signal assignments, and $^{13}$C{$^1$H} INEPT and CP-MAS for the selective detection of mobile and rigid groups, respectively, provided a fine picture of the dynamics of the surfactant aggregates where the ethylene oxide groups appear to be in close interaction with clay mineral surface. The location of the hydrophilic headgroups near the clay surface was corroborated by $^1$H

and $^1$H{$^{27}$Al}} NMR experiments that allowed us to get information in a site-specific manner and gives access to dimensions characteristic of the surfactant aggregates and beyond the usual range probed by solid state NMR. Finally, $^{23}$Na NMR in association with $^1$H NMR experiments measurements ruled out the possibility that H bonds play a significant role in the interactions between the clay host and the intercalated nonionic surfactants. The whole NMR results support ion-dipole interaction around Na$^+$ exchangeable cations as the main driving force in the adsorption of $C_{10}E_3$ and more generally of nonionic compounds onto swelling clay minerals.
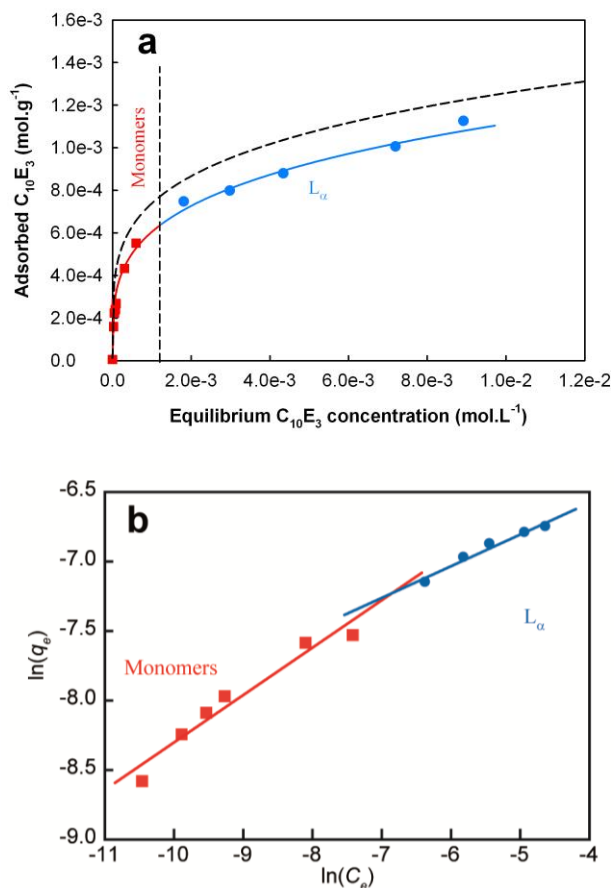
## Acknowledgments

# Figures



**Figure 1.** (a) Adsorption isotherms at the equilibrium of $C_{10}E_3$ onto both a synthetic Na exchanged montmorillonite (Na-S-Mt, full line) where both monomers and L domains can be identified in red and blue respectively, and its natural analogous (dashed black line, adapted from). (b) the fitting obtained with the use of a Langmuir model applied in both monomers (red line) and a lamellar phase onto Na-S-Mt respectively where the adsorption mechanisms involved cohesion forces between alkyl chains driving t o a bilayer aggregation onto a clay surface.
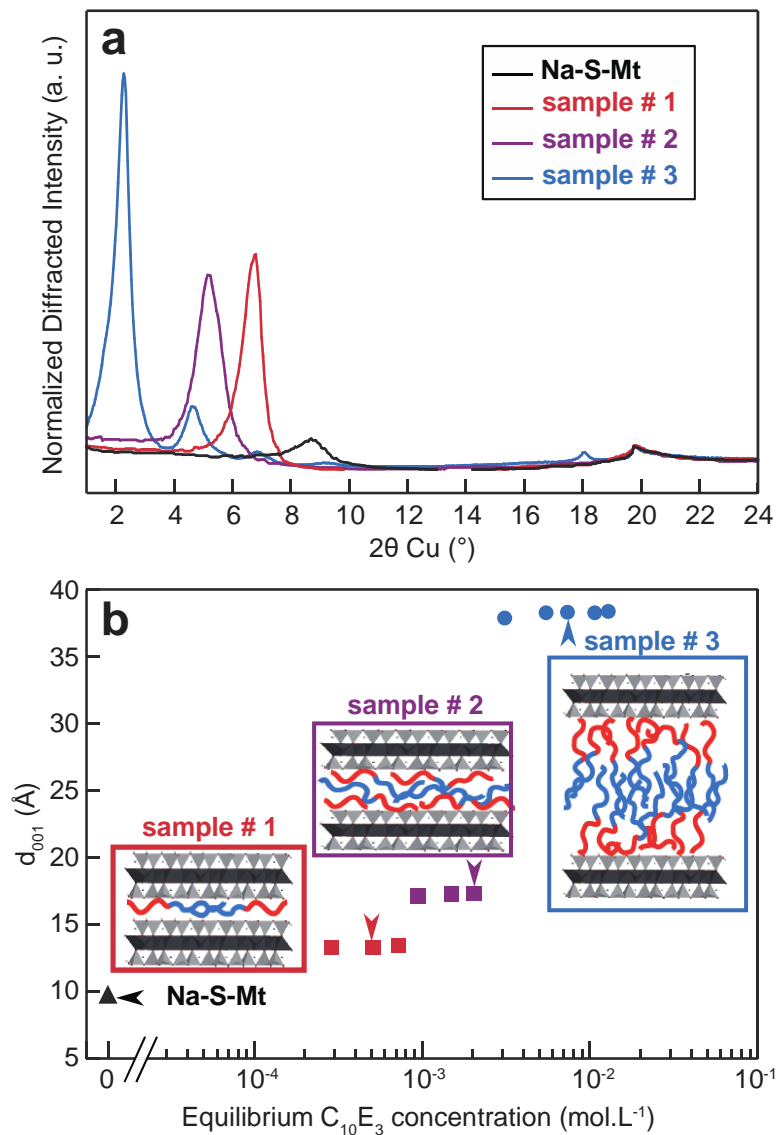
R. Guégan et al.

**Figure 2.** X-ray diffraction patterns collected for Na-Mt (in black) and Mt-$C_{10}E_3$ organoclay samples prepared with initial $C_{10}E_3$ concentrations of $5\times10^{-4}$, $2\times10^{-3}$, and $7.5\times10^{-3}$ mol.$L^{-1}$ (in red – sample # 1, purple - sample # 2 - and blue - sample # 3, respectively). (b) Evolution of the basal distance measured from the *001* reflections of the X-ray diffractograms, which show three distinct types of surfactant organizations within the inter-layer space.
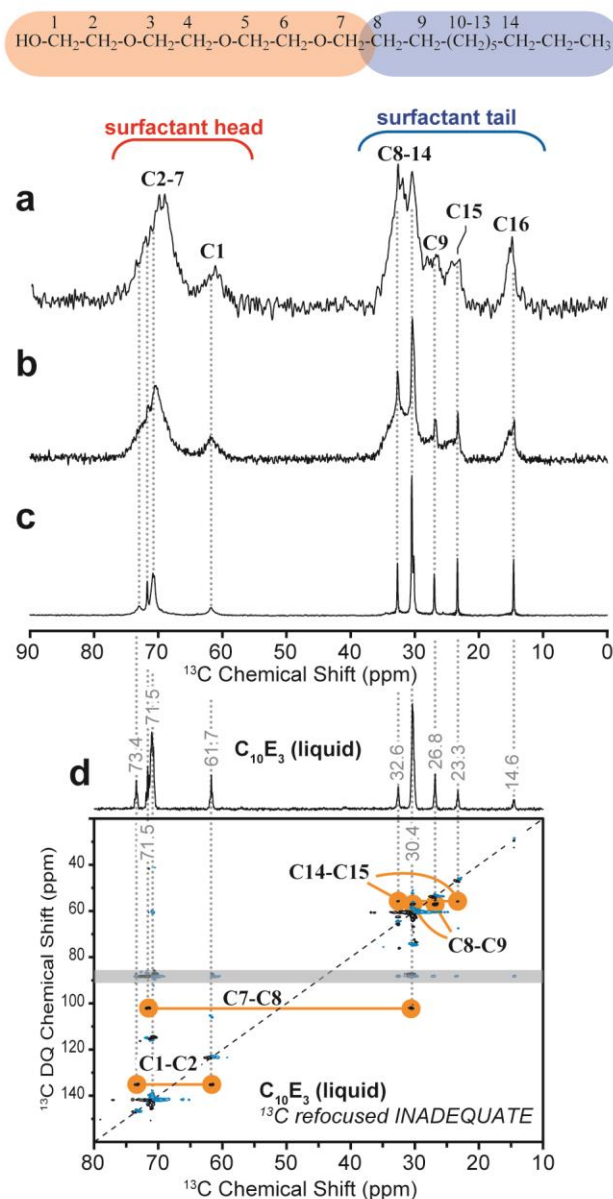
R. Guégan et al.

**Figure 3.** Solid-state $^{13}$C NMR spectra of Mt-$C_{10}E_3$ organoclay samples # (a) 1, (b) 2, and (c) 3 prepared with initial surfactant concentrations of $5\times10^{-4}$, $2\times10^{-3}$, and $7.5\times10^{-3}$ mol.L$^{-1}$, respectively. Peak labeling refers to the C-site labeling shown on the surfactant formula shown on top. The assignment was verified using the solution-state $^{13}$C-$^{13}$C correlation NMR spectrum shown in (d), collected on the raw surfactant with the refocused INADEQUATE pulse sequence. Positive and negative contours are shown in black and blue, respectively. The gray region indicates experimental artifacts. Pairs of cross-peaks highlighted in orange indicate C-C bonds between different carbon sites along the chain.
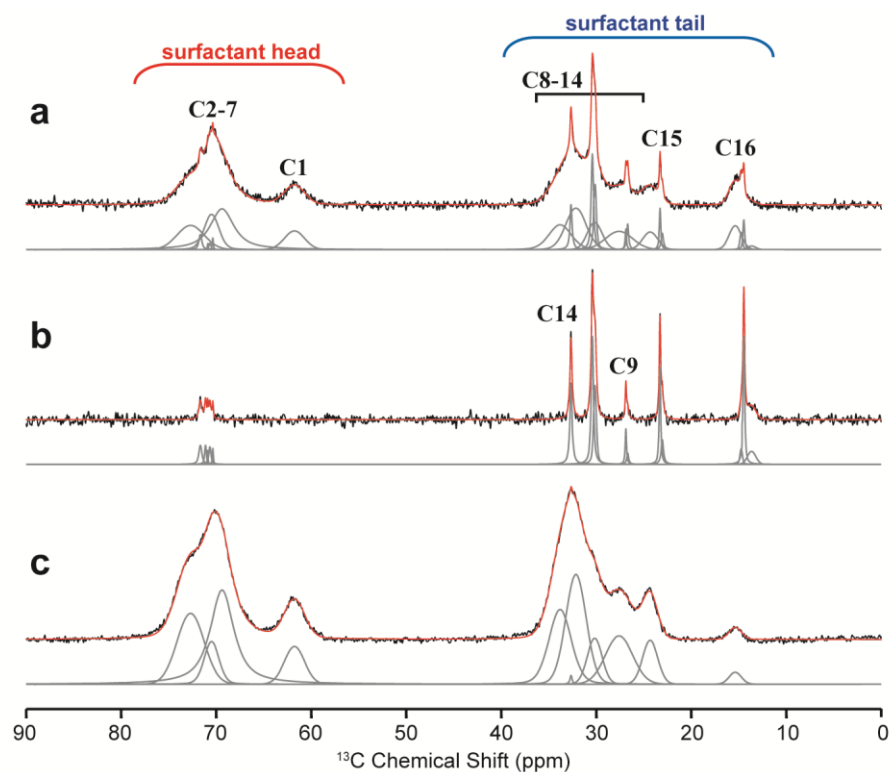
R. Guégan et al.

**Figure 4.** Different types of $^{13}$C solid-state NMR spectra collected for the Mt-C$_{10}$E$_3$ organoclay sample # 2, prepared with an initial surfactant concentration of $2\times10^{-3}$ mol.L$^{-1}$, to generate contrast between $^{13}$C NMR peaks based on the corresponding site mobilities. (a) Quantitative $^{13}$C spectrum. (b) liquid-state-type $^{13}$C$\{^{1}$H$\}$ refocused INEPT experiment showing selectively the mobile surfactant fractions. (c) Solid-state $^{13}$C$\{^{1}$H$\}$ CP-MAS experiment collected with a short contact time to emphasize rigid surfactant fractions. The models and corresponding individual components shown in grey below were obtained with a simultaneous fit all three spectra using a single set of peak positions, widths and shapes.
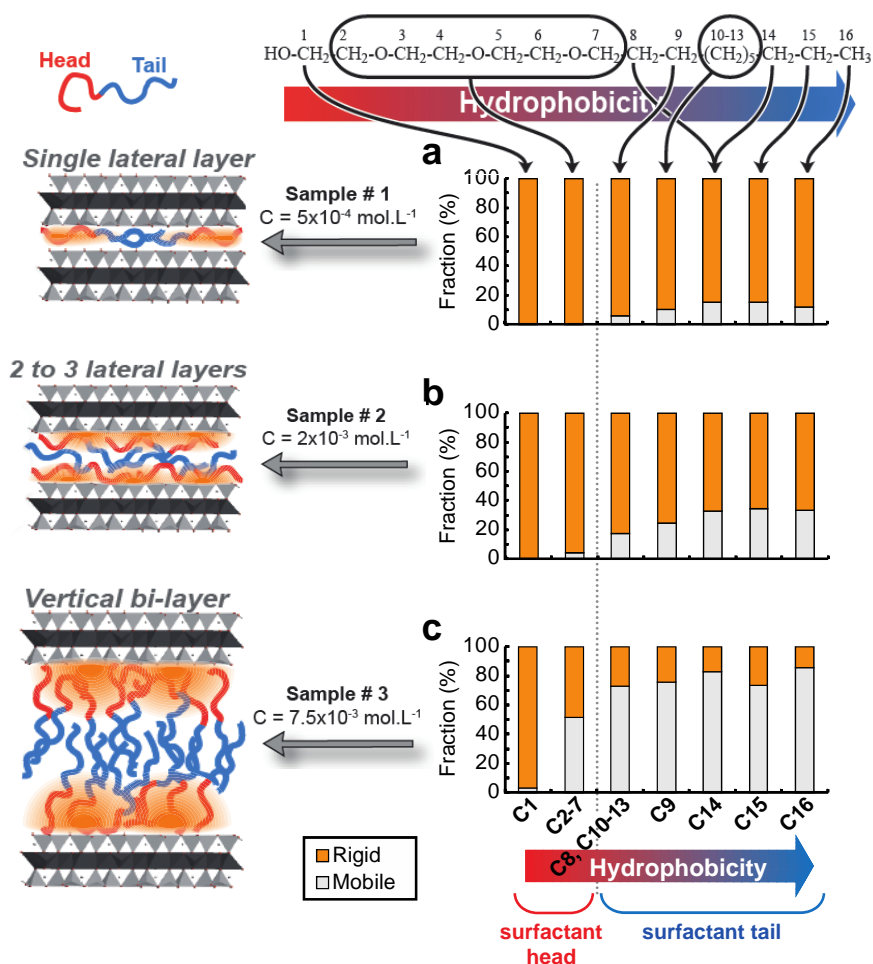
R. Guégan et al.

**Figure 5.** Fractions of (orange) rigid and (pale gray) mobile carbon sites measured from quantitative $^{13}$C NMR spectra for Mt-C$_{10}$E$_3$ organoclay samples # (a) 1, (b) 2, and (c) 3 prepared with initial surfactant concentrations of $5\times10^{-4}$, $2\times10^{-3}$, and $7.5\times10^{-3}$ mol.L$^{-1}$, respectively.

R. Guégan et al.

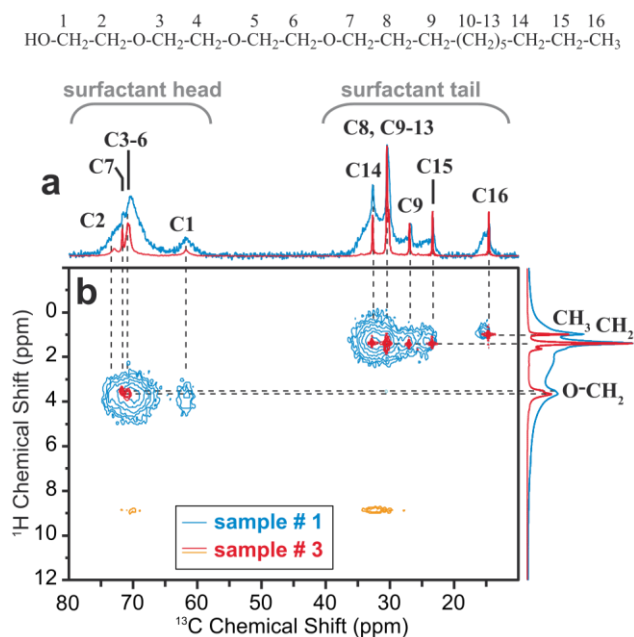**Figure 6.** $^{13}C\{^1H\}$ 2D correlation NMR spectra collected for Mt-C$_{10}$E$_3$ organoclay samples # 1 (in blue) and 3 (in red) prepared with initial surfactant concentrations of $5\times10^{-4}$ and $7.5\times10^{-3}$ mol.L$^{-1}$, respectively. The blue spectrum is a solid-state-type HETCOR spectrum probing C-H spatial proximities and using a short contact time to be selective of bonded C-H pairs in rigid surfactant moieties. The spectrum in red (with negative contours in orange) is a liquid-state-type refocused INEPT experiment probing C-H bonds in mobile surfactant moieties. 1D spectra shown on top and on the right are quantitative $^{13}$C and $^1$H NMR spectra, respectively.
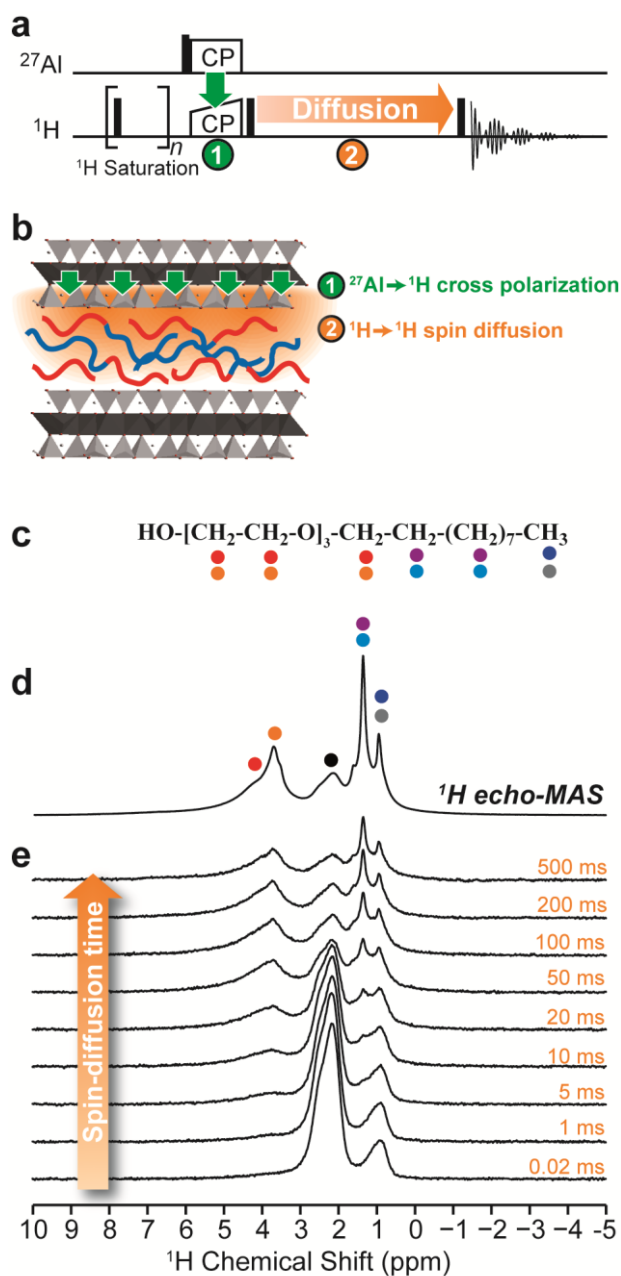
R. Guégan et al.

**Figure 7.** (a) NMR sequence of radio-frequency pulses designed to probe nanometric proximities between Al sites of the clay host and $^1$H nuclei of organic guest molecules as illustrated in the schematic in (b) (see details in text). (c) $C_{10}E_3$ formula with the color code used to label the different $^1$H NMR peaks identified in the quantitative $^1$H MAS NMR spectrum shown in (d). (e) Series of $^1$H{$^{27}$Al} NMR experiments collected for sample # 2 ([$C_{10}E_3$] = $2.0 \times 10^{-3}$ mol.$L^{-1}$) with the pulse sequence shown in (a) and using different durations of the $^1$H-$^1$H spin-diffusion mixing time (step 2 in (a)) to propagate the $^1$H magnetization from the clay hydroxyl groups to different fragments of the intercalated surfactant molecules.
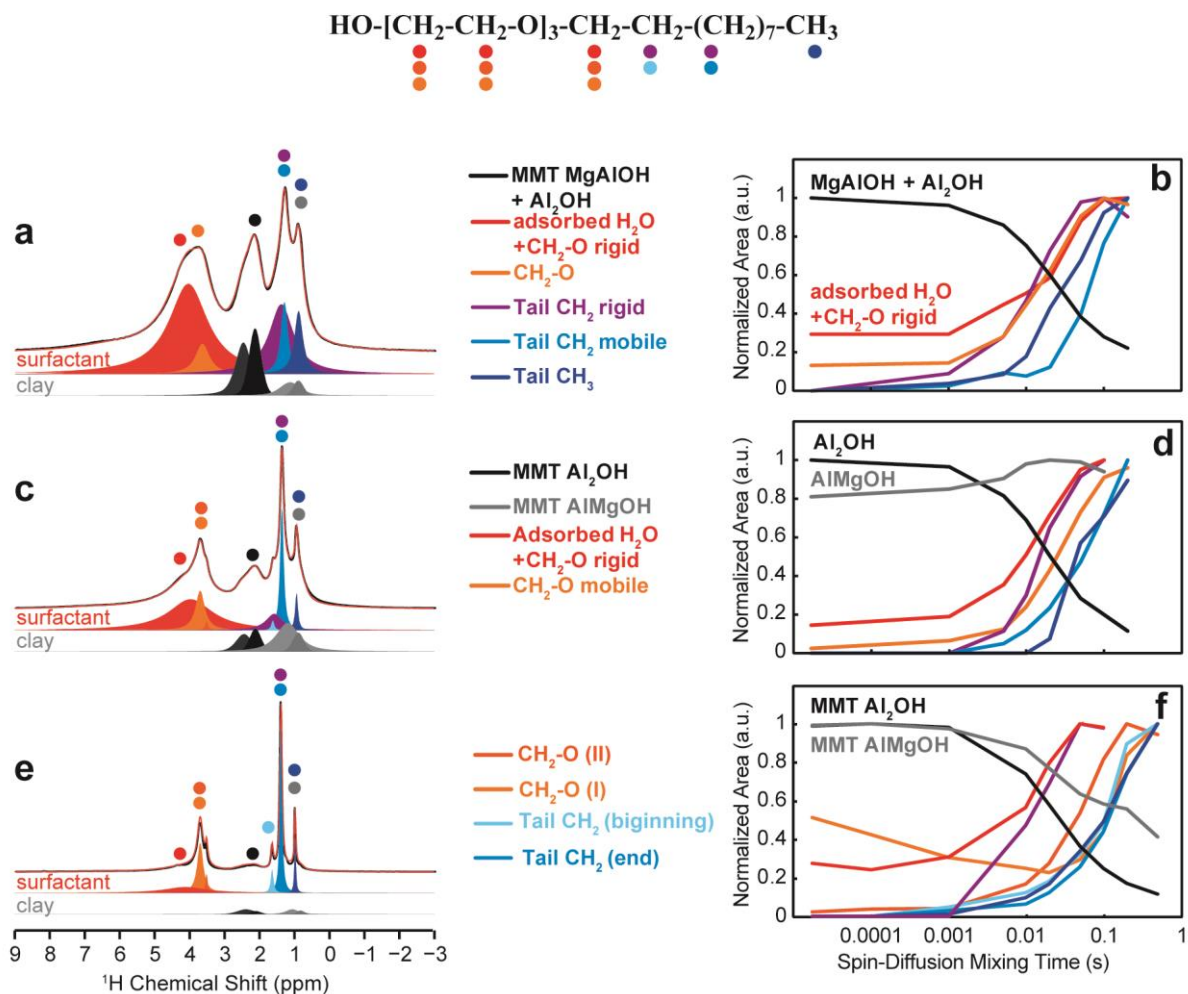
R. Guégan et al.

20

**Figure 8.** (a,c,e) Quantitative $^1$H NMR spectra (in black) with the corresponding model (in red) and individual components (same color code as in Fig. 8) for Mt-C$_{10}$E$_3$ organoclay samples # (a) 1, (c) 2, and (e) 3 prepared with initial surfactant concentrations of 5×10$^{-4}$, 2×10$^{-3}$, and 7.5×10$^{-3}$ mol.L$^{-1}$, respectively. (b,d,f) Normalized intensities measured for all individual components using the experiment described in Figure 8, and plotted as functions of the $^1$H-$^1$H spin-diffusion mixing time during which the $^1$H magnetization diffuses from clay hydroxyl sites to the surfactant $^1$H nuclei.
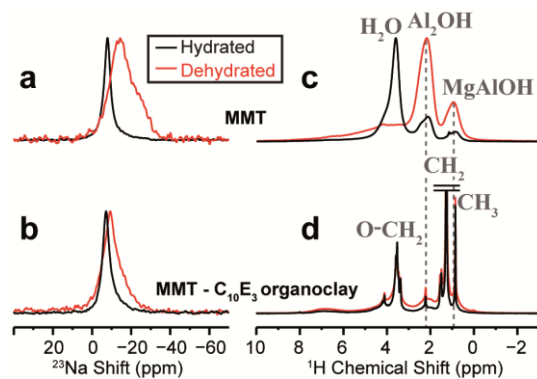
R. Guégan et al.

**Figure 9.** Solid-state (a,b) $^{23}$Na and (b,c) $^{1}$H MAS NMR spectra collected at room temperature (a,c) for the reference Na-Mt sample and (b,d) for MMT-C$_{10}$E$_3$ organoclay sample prepared with initial surfactant concentrations of $7.5 \times 10^{-3}$ mol.L$^{-1}$. Spectra in black and red were obtained on as-made and dehydrated samples, respectively. The intense $^{1}$H NMR signals due to mobile CH$_2$ groups are truncated in (d) to better reveal differences among smaller spectral components.

R. Guégan et al.

# References

1.      Heinz, H.; Suter, U. W., Surface Structure of Organoclays. *Angewandte Chemie International Edition* **2004,** 43, (17), 2239-2243.

2.      Richard, C.; Balavoine, F.; Schultz, P.; Ebbesen, T. W.; Mioskowski, C., Supramolecular Self-Assembly of Lipid Derivatives on Carbon Nanotubes. *Science* **2003,** 300, (5620), 775-778.

3.      Srinivas, G.; Nielsen, S. O.; Moore, P. B.; Klein, M. L., Molecular Dynamics Simulations of Surfactant Self-Organization at a Solidâˆ'Liquid Interface. *Journal of the American Chemical Society* **2005,** 128, (3), 848-853.

4.      Grant, L. M.; Ducker, W. A., Effect of Substrate Hydrophobicity on Surface‚àíAggregate Geometry:‚Äâ Zwitterionic and Nonionic Surfactants. *The Journal of Physical Chemistry B* **1997,** 101, (27), 5337-5345.

5.      Cadars, S.; Guégan, R.; Garaga, M. N.; Bourrat, X.; Le Forestier, L.; Fayon, F.; Huynh, T. V.; Allier, T.; Nour, Z.; Massiot, D., New Insights into the Molecular Structures, Compositions, and Cation Distributions in Synthetic and Natural Montmorillonite Clays. *Chemistry of Materials* **2012,** 24, (22), 4376-4389.

6.      Ferrage, E.; Lanson, B.; Sakharov, B. A.; Drits, V. A., Investigation of smectite hydration properties by modeling experimental X-ray diffraction patterns: Part I. Montmorillonite hydration properties. *American Mineralogist* **2005,** 90, (8-9), 1358-1374.

7.      Guégan, R.; Gautier, M.; Beny, J.-M.; Muller, F., ADSORPTION OF A C10E3 NON-IONIC SURFACTANT ON A Ca-SMECTITE. *Clays and Clay Minerals* **2009,** 57, (4), 502-509.

8.      Karaborni, S.; Smit, B.; Heidug, W.; Urai, J.; van Oort, E., The Swelling of Clays: Molecular Simulations of the Hydration of Montmorillonite. *Science* **1996,** 271, (5252), 1102-1104.

9.      Ohkubo, T.; Saito, K.; Kanehashi, K.; Ikeda, Y., A study on hydration behaviors of interlayer cations in montmorillonite by solid state NMR. *Science and Technology of Advanced Materials* **2004,** 5, (5-6), 693-696.

10.     Rosen, M. J., *Surfactants and interfacial phenomena / Milton J. Rosen*. Wiley: New York, 1978.

11.     Deng, Y.; Dixon, J.; White, G. N., Bonding mechanisms and conformation of poly(ethylene oxide)-based surfactants in interlayer of smectite. *Colloid Polym Sci* **2006,** 284, (4), 347-356.

12.     Deng, Y. D., J.B.; White, G.N., Intercalation and surface modification of smectite by two non-ionic surfactants. *Clays and Clay Minerals* **2003,** 51, 150-161.

13.     Finocchio, E.; Baccini, I.; Cristiani, C.; Dotelli, G.; Gallo Stampino, P.; Zampori, L., Hybrid Organo‚ÄìInorganic Clay with Nonionic Interlayers. Mid- and Near-IR Spectroscopic Studies. *The Journal of Physical Chemistry A* **2011,** 115, (26), 7484-7493.

14.     Su, C.-C.; Shen, Y.-H., Adsorption of poly(ethylene oxide) on smectite: Effect of layer charge. *Journal of Colloid and Interface Science* **2009,** 332, (1), 11-15.

15.     Zhuang, G.; Zhang, Z.; Guo, J.; Liao, L.; Zhao, J., A new ball milling method to produce organo-montmorillonite from anionic and nonionic surfactants. *Applied Clay Science* **2015,** 104, 18-26.

.16.    Guegan, R., Self-assembly of a non-ionic surfactant onto a clay mineral for the preparation of hybrid layered materials. *Soft Matter* **2013,** 9, (45), 10913-10920.

17.     Guegan, R.; Sueyoshi, K.; Anraku, S.; Yamamoto, S.; Miyamoto, N., Sandwich organization of non-ionic surfactant liquid crystalline phases as induced by large inorganic K4Nb6O17 nanosheets. *Chemical Communications* **2016,** 52, (8), 1594-1597.

18.     Guégan, R., Intercalation of a Nonionic Surfactant (C10E3) Bilayer into a Na-Montmorillonite Clay. *Langmuir* **2010,** 26, (24), 19175-19180.

19.     Levitz, P.; Van Damme, H.; Keravis, D., Fluorescence decay study of the adsorption of nonionic surfactants at the solid-liquid interface. 1. Structure of the adsorption layer on a hydrophilic solid. *The Journal of Physical Chemistry* **1984,** 88, (11), 2228-2235.

20.     Breen, C.; Rawson, J. O.; Mann, B. E.; Aston, M., In situ 133Cs and 1H solution-phase NMR, thermoanalytical and X-ray diffraction studies of the adsorption of polyalkyleneglycol on Texas bentonite. *Colloids and Surfaces A: Physicochemical and Engineering Aspects* **1998,** 132, (1), 17-30.

21.     Grandjean, J., Interaction of Poly(ethylene glycol) Monoalkyl Ethers with Synthetic Saponites in Aqueous Suspensions:‚Äâ A Multinuclear Magnetic Resonance Study. *Langmuir* **1998,** 14, (5), 1037-1040.

22.     Hrobarikova, J.; Robert, J. L.; Calberg, C.; J√©r√¥me, R.; Grandjean, J., Solid-State NMR Study of Intercalated Species in Poly(Œµ-caprolactone)/Clay Nanocomposites. *Langmuir* **2004,** 20, (22), 9828-9833.

23.     Kubies, D.; Jérome, R.; Grandjean, J., Surfactant Molecules Intercalated in Laponite as Studied by 13C and 29Si MAS NMR. *Langmuir* **2002,** 18, (16), 6159-6163.

24.     Mirau, P. A.; Serres, J. L.; Jacobs, D.; Garrett, P. H.; Vaia, R. A., Structure and Dynamics of Surfactant Interfaces in Organically Modified Clays. *The Journal of Physical Chemistry B* **2008,** 112, (34), 10544-10551.

25.     Panek, G.; Schleidt, S.; Mao, Q.; Wolkenhauer, M.; Spiess, H. W.; Jeschke, G., Heterogeneity of the Surfactant Layer in Organically Modified Silicates and Polymer/Layered Silicate Composites. *Macromolecules* **2006,** 39, (6), 2191-2200.

26.     Kharkov, B. B.; Dvinskikh, S. V., Chain dynamics of surfactants in mesoporous silica. *Physical Chemistry Chemical Physics* **2013,** 15, (42), 18620-18626.

27.     Kharkov, B. B.; Dvinskikh, S. V., Conformational Dynamics of Surfactant in a Mesolamellar Composite Studied by Local Field NMR Spectroscopy. *The Journal of Physical Chemistry C* **2013,** 117, (46), 24511-24517.

28.     Kharkov, B. B.; Corkery, R. W.; Dvinskikh, S. V., Phase Transitions and Chain Dynamics of Surfactants Intercalated into the Galleries of Naturally Occurring Clay Mineral Magadiite. *Langmuir* **2014,** 30, (26), 7859-7866.

29.     Kharkov, B. B.; Chizhik, V. I.; Dvinskikh, S. V., Probing Molecular Mobility in Nanostructured Composites by Heteronuclear Dipolar NMR Spectroscopy. *The Journal of Physical Chemistry C* **2014,** 118, (48), 28308-28313.

30.     Ferreira, T. M.; Bernin, D.; Topgaard, D., NMR Studies of Nonionic Surfactants. *Annual Reports on NMR Spectroscopy* **2013,** 79, 73-127.

31.     Cadars, S.; Layrac, G.; Gérardin, C.; Deschamps, M.; Yates, J. R.; Tichit, D.; Massiot, D., Identification and Quantification of Defects in the Cation Ordering in Mg/Al Layered Double Hydroxides. *Chemistry of Materials* **2011,** 23, (11), 2821-2831.

32.     Simpson, A. J.; Simpson, M. J.; Kingery, W. L.; Lefebvre, B. A.; Moser, A.; Williams, A. J.; Kvasha, M.; Kelleher, B. P., The Application of 1H High-Resolution Magic-Angle Spinning NMR for the Study of Clay‚àíOrganic Associations in Natural and Synthetic Complexes. *Langmuir* **2006,** 22, (10), 4498-4503.

33.     Le Forestier, L.; Muller, F.; Villieras, F.; Pelletier, M., Textural and hydration properties of a synthetic montmorillonite compared with a natural Na-exchanged clay analogue. *Applied Clay Science* **2010,** 48, (1‚Äì2), 18-25.

34.     Guégan, R., Confinement effects on water structure in membrane lyotropic phases. *Journal of Colloid and Interface Science* **2011,** 358, (2), 485-490.

35.     Corkill, J. M.; Goodman, J. F.; Harrold, S. P., Thermodynamics of micellization of non-ionic detergents. *Transactions of the Faraday Society* **1964,** 60, 202-207.

36.     Bielecki, A.; Kolbert, A. C.; De Groot, H. J. M.; Griffin, R. G.; Levitt, M. H., Frequency-Switched Lee—Goldburg Sequences in Solids. *Advances in Magnetic and Optical Resonance* **1990,** 14, 111-124.

37.     Burum, D. P.; Ernst, R. R., Net polarization transfer via a J-ordered state for signal enhancement of low-sensitivity nuclei. *Journal of Magnetic Resonance (1969)* **1980,** 39, (1), 163-168.

38.     Nakai, T.; McDowell, C. A., One- and Two-Dimensional Refocused INADEQUATE NMR Experiments. *Journal of Magnetic Resonance, Series A* **1993,** 104, (2), 146-153.

39.     Benn, R.; Grondey, H.; Brevard, C.; Pagelot, A., The detection of connectivities of rare spin-1/2 nuclei in the solid state using natural abundance samples: 13C and 29Si INADEQUATE and COSY type experiments. *Journal of the Chemical Society, Chemical Communications* **1988**, (2), 102-103.

40.     Cases, J. M.; Villieras, F., Thermodynamic model of ionic and nonionic surfactants adsorption-abstraction on heterogeneous surfaces. *Langmuir* **1992,** 8, (5), 1251-1264.

41.     Levitz, P., Aggregative adsorption of nonionic surfactants onto hydrophilic solid/water interface. Relation with bulk micellization. *Langmuir* **1991,** 7, (8), 1595-1608.

42.     LeVan, M. D.; Vermeulen, T., Binary Langmuir and Freundlich isotherms for ideal adsorbed solutions. *The Journal of Physical Chemistry* **1981,** 85, (22), 3247-3250.

43.     Ferreira, T. M.; Medronho, B.; Martin, R. W.; Topgaard, D., Segmental order parameters in a nonionic surfactant lamellar phase studied with 1H-13C solid-state NMR. *Physical Chemistry Chemical Physics* **2008,** 10, (39), 6033-6038.

44.     Nowacka, A.; Mohr, P. C.; Norrman, J.; Martin, R. W.; Topgaard, D., Polarization Transfer Solid-State NMR for Studying Surfactant Phase Behavior. *Langmuir* **2010,** 26, (22), 16848-16856.

45.     Nowacka, A.; Bongartz, N. A.; Ollila, O. H. S.; Nylander, T.; Topgaard, D., Signal intensities in 1H–13C CP and INEPT MAS NMR of liquid crystals. *Journal of Magnetic Resonance* **2013,** 230, 165-175.

46.     Szczerba, M.; Kłapyta, Z.; Kalinichev, A., Ethylene glycol intercalation in smectites. Molecular dynamics simulation studies. *Applied Clay Science* **2014,** 91–92, 87-97.

47.     Cygan, R. T.; Liang, J.-J.; Kalinichev, A. G., Molecular Models of Hydroxide, Oxyhydroxide, and Clay Phases and the Development of a General Force Field. *The Journal of Physical Chemistry B* **2004,** 108, (4), 1255-1266.

48.     Kalinichev, A. G.; Padma Kumar, P.; James Kirkpatrick, R., Molecular dynamics computer simulations of the effects of hydrogen bonding on the properties of layered double hydroxides intercalated with organic acids. *Philosophical Magazine* **2010,** 90, (17-18), 2475-2488.

49.     Cygan, R. T.; Greathouse, J. A.; Heinz, H.; Kalinichev, A. G., Molecular models and simulations of layered materials. *Journal of Materials Chemistry* **2009,** 19, (17), 2470-2481.

50.     Krishnan, M.; Saharay, M.; Kirkpatrick, R. J., Molecular Dynamics Modeling of CO2 and Poly(ethylene glycol) in Montmorillonite: The Structure of Clay–Polymer Composites and the Incorporation of CO2. *The Journal of Physical Chemistry C* **2013,** 117, (40), 20592-20609.

51.     Alonso, B.; Fayon, F.; Massiot, D.; Amenitsch, H.; Malfatti, L.; Kidchob, T.; Costacurta, S.; Innocenzi, P., Hybrid Organic-Inorganic Mesostructured Membranes: Interfaces and Organization at Different Length Scales. *Journal of Physical Chemistry C* **2010,** 114, (27), 11730-11740.

52.     Baccile, N.; Laurent, G.; Bonhomme, C.; Innocenzi, P.; Babonneau, F., Solid-State NMR Characterization of the Surfactant−Silica Interface in Templated Silicas: Acidic versus Basic Conditions. *Chemistry of Materials* **2007,** 19, (6), 1343-1354.

53.     Jeffrey, G. A.; Yeon, Y., The correlation between hydrogen-bond lengths and proton chemical shifts in crystals. *Acta Crystallographica Section B* **1986,** 42, (4), 410-413.

54.     Bo, B.; Robert, W. V., Correlations between proton chemical shift tensors, deuterium quadrupole couplings, and bond distances for hydrogen bonds in solids. *The Journal of Chemical Physics* **1980,** 73, (5), 2037-2043.

55.     Xue, X.; Kanzaki, M., Correlations between 29Si, 17O and 1H NMR properties and local structures in silicates: an ab initio calculation. *Physics and Chemistry of Minerals* **1998,** 26, (1), 14-30.

56.     Tielens, F.; Gervais, C.; Lambert, J. F.; Mauri, F.; Costa, D., Ab Initio Study of the Hydroxylated Surface of Amorphous Silica: A Representative Model. *Chemistry of Materials* **2008,** 20, (10), 3336-3344.

57.     Ferreira, T. M.; Topgaard, D.; Ollila, O. H. S., Molecular Conformation and Bilayer Pores in a Nonionic Surfactant Lamellar Phase Studied with 1H–13C Solid-State NMR and Molecular Dynamics Simulations. *Langmuir* **2014,** 30, (2), 461-469.